ELSEVIER

Journal of Hazardous Materials B137 (2006) 1838–1847

Journal of Hazardous Materials

www.elsevier.com/locate/jhazmat

Effects of Fe-doping on the photocatalytic activity of mesoporous TiO_2 powders prepared by an ultrasonic method

Minghua Zhou [a,b], Jiaguo Yu [a,*], Bei Cheng [a]

[a] *State Key Laboratory of Advanced Technology for Material Synthesis and Processing, Wuhan University of Technology, Luoshi Road 122, Wuhan 430070, PR China*

[b] *Staff Room of Chemistry, Yunyang Medical College, Shiyan, 442000 Hubei, PR China*

Received 12 April 2006; received in revised form 6 May 2006; accepted 8 May 2006

Available online 16 May 2006

Abstract

Highly photoactive nanocrystalline mesoporous Fe-doped TiO_2 powders were prepared by the ultrasonic-induced hydrolysis reaction of tetrabutyl titanate ($Ti(OC_4H_9)_4$) in a ferric nitrate aqueous solution (pH 5) without using any templates or surfactants. The as-prepared samples were characterized by thermogravimetry and differential thermal analysis (TG-DTA), X-ray diffraction (XRD), N_2 adsorption–desorption measurements, UV–visible adsorbance spectra (UV–vis) and X-ray photoelectron spectroscopy (XPS). The photocatalytic activities were evaluated by the photocatalytic oxidation of acetone in air. The results showed that all the Fe-doped TiO_2 samples prepared by ultrasonic methods were mesoporous nanocrystalline. A small amount of Fe^{3+} ions in TiO_2 powders could obviously enhance their photocatalytic activity. The photocatalytic activity of Fe-doped TiO_2 powders prepared by this method and calcined at 400 °C exceeded that of Degussa P25 (P25) by a factor of more than two times at an optimal atomic ratio of Fe to Ti of 0.25. The high activities of the Fe-doped TiO_2 powders could be attributed to the results of the synergetic effects of Fe-doping, large BET specific surface area and small crystallite size.

Keywords: Fe-doping; Mesoporous; Nanocrystalline; Ultrasonic-induced; Acetone; Photocatalytic activity; Visible light

1. Introduction

During the past decade, various catalytic techniques have been investigated to solve the increasingly serious environmental pollution problems. Heterogeneous photocatalysis is a popular technique that has great potential to control aqueous contaminates or air pollutants. Among various oxide semiconductor photocatalysts, titanium dioxide has been proved to be the most suitable photocatalysts for widespread environmental application because of its biological and chemical inertness, strong oxidizing power, nontoxicity and long-term stability against photo and chemical corrosion [1–9]. However, TiO_2 can be activated only under UV light of wavelengths < 387 nm irradiation due to its large band gap of 3.2 eV. The solar spectrum usually contains about 4% UV light. Owing to this inherent limitation, the solar energy cannot be utilized efficiently in the photocatalytic process [10,11].

The photocatalytic activity of TiO_2 usually depends on a competition between the following two processes, that is, the ratio of the transfer rate of surface charge carriers from the interior to the surface to the recombination rate of photo-generated electrons and holes. If the recombination of photo-generated electrons and holes occurs too fast (<0.1 ns), then there is not enough time for any other chemical reaction to occur. Compared with other semiconductor, the surface charge carriers of TiO_2 are relatively long-lived (around 250 ns), allowing the electrons or holes to travel to the crystallite surface. It is on the TiO_2 surface that different types of radicals are formed. The most common radicals are the OH radicals, which are then free to carry out other chemical reactions on the surface of TiO_2 [12,13]. In order to extend its light absorption moving into visible-light region, and also to reduce the recombination of photo-generated electrons and holes, various metal and nonmetal ions have been doped into TiO_2 [14–19]. For example, Choi et al. conducted a systematic study of metal ions doping into TiO_2 for 21 metal ions. Among various transition metal ions, they considered that the Fe^{3+} was proved to be a successful doping element due to its half-filled electronic configuration. It has been reported that a proper con-

* Corresponding author. Tel.: +86 27 87883610; fax: +86 27 87870261.
E-mail address: jiaguoyu@yahoo.com (J. Yu).

0304-3894/$ – see front matter © 2006 Elsevier B.V. All rights reserved.
doi:10.1016/j.jhazmat.2006.05.028

centration of Fe^{3+} ions in TiO_2 is not only to favor electron–hole separation, but also to narrow its band gap [2,6,15,20].

The photocatalytic activity of TiO_2 must be further enhanced from the point of views of practical use and commerce. In order to achieve this purpose, mesoporous TiO_2 has attracted much attention due to its high specific surface area and pore volume. The mesoporous materials have been successfully synthesized via many conventional approaches with the aid of surfactants as templates based on a liquid crystal template mechanism [21]. However, this method often requires a long time and multiple-step procedures. Sonochemistry has been proven to be an excellent method in the preparation of mesoporous materials [22–24], which arises from acoustic cavitations, the formation, growth, and implosive collapse of bubbles in a liquid. The collapse of bubbles generates localized hot spots with transient temperatures of above 5000 K, pressure of about 20 MPa, and heating and cooling rates greater than 10^9 K s^{-1}. These extreme conditions can obviously accelerate the hydrolysis or condensation reaction. In our previous work [25], we prepared high-photoactivity mesoporous TiO_2 powders by the ultrasonic method without using any templates or surfactants. Herein, we utilized for the first time the ultrasonic method to synthesize highly photoactive nanocrystalline mesoporous Fe-doped TiO_2 powders.

2. Experimental

2.1. Synthesis

Tetrabutyl titanate ($Ti(OC_4H_9)_4$, TBOT) was used as a titanium source. TBOT (8.8 ml) was added dropwise to a 40 ml ferric nitrate aqueous solution (the atomic ratios of Fe to Ti = 0, 0.05, 0.25, 0.50, 2.50 nominal atomic% (at.%)) with pH 5 in a 100 ml beaker under irradiated with a high intensity ultrasonic horn (KS-1200, China, 6.3 mm diameter Ti-horn, 20 KHz, and 1200 W/cm^2 at 50% efficiency) for 45 min at thermostatic bath about 20 °C. In order to eliminate the effect of pH, we choose the pH of 0.015 M ferric nitrate aqueous solution (the Fe/Ti ratio = 2.50 at.%) as a standard value (about pH 5). Other ferric nitrate solutions were adjusted to pH 5 with dilute nitrate acid. The ultrasonic system is 2 s on and 2 s off in air during the whole reaction. After ultrasonic reaction, the precipitate was centrifuged and washed with distilled water and alcohol for three times. Then the wet gel was dried under vacuum at 80 °C for about 10 h. The obtained white xerogel was labeled as US80-*x*. The *x* denoted the atomic ratio of Fe/Ti (at.%). The obtained white xerogel was calcined at 400 °C in air for 3 h and the calcined powders were labeled as US400-*x*. To further investigate the effects of calcined temperatures on the physical and chemical properties of the as-prepared catalysts, the sample US80-0.25 was also calcined at 200, 300, 400, 500, 600 °C in air for 3 h, respectively.

2.2. Characterization

The crystallization behaviors of the as-prepared powders were monitored with a DTA-TG instrument (Netzsch STA 449C). It performed in airflow of 100 ml min^{-1} at a heating rate 10 °C min^{-1} from room temperature to 900 °C. X-ray diffraction (XRD) patterns obtained on an X-ray diffractometer (type HZG41B-PC) with Cu Kα radiation at a scan rate (θ) of 0.05° s^{-1} were used to determine the identity of any phase present and their crystallite size. The accelerating voltage and the applied current were 15 kV and 20 mA, respectively. The Brunauer–Emmett–Teller (BET) surface area (S_{BET}) of the powders was analyzed by nitrogen adsorption in an AUTOSORB-1 (Quantachrome Instruments, USA) nitrogen adsorption apparatus. The as-prepared xerogel sample was degassed at 80 °C and all the calcined samples and Degussa P25 (P25) were degassed at 180 °C prior to nitrogen adsorption measurements. The BET surface area was determined by multipoint BET method using the adsorption data in the relative pressure (P/P_0) range of 0.05–0.3. Desorption isotherm was used to determine the pore size distribution using the Barret–Joyner–Halender (BJH) method with cylindrical pore size [26]. The nitrogen adsorption volume at the relative pressure (P/P_0) of 0.994 was used to determine the pore volume and average pore size. UV–visible adsorbance spectra of as-prepared TiO_2 powders were obtained for the dry-pressed disk samples with a UV–visible spectrophotometer (UV2550, Shimadzu, Japan). $BaSO_4$ was used as an adsorbance standard in the UV–visible adsorbance experiment. X-ray photoelectron spectroscopy (XPS) measurements were done on a Kratos XSAM800 XPS system with Cu Kα source. All the binding energies were referenced to C1s peak at 284.80 eV of the surface adventitious carbon.

2.3. Measurement of photocatalytic activity

Acetone, formaldehyde and other volatile organic compounds (VOCs) are common indoor air pollutants in modern houses, which have been the subject of numerous complaints regarding health disorders, such as leukemia, nausea, headache and fatigue [27,28]. These volatile harmful gases usually come from the plywood, particleboard and adhesives for wall clothes, which have been used in construction and furnishing. In order to improve indoor air quality (IAQ), these volatile organic compounds (VOCs) must be eliminated. In our previous work [25], we found that choosing acetone as a model contaminate was more reasonable than formaldehyde. Therefore, in this work, we choose the acetone as a model contaminates to evaluate the photocatalytic activity of the as-prepared nanocrystalline mesoporous Fe-doped TiO_2 powders. Photocatalytic oxidation acetone is based on the following reactions [29,30]:

$$CH_3COCH_3 + 4O_2 \rightarrow 3CO_2 + 3H_2O \quad (1)$$

The photocatalytic activity experiments of the as-prepared powders and P25 for the oxidation of acetone in air were performed at ambient temperature with a 15 l photocatalytic reactor. The catalysts were prepared by coating an aqueous suspension of TiO_2 powders onto three dishes with a diameter of about 9.0 cm. The weight of catalysts used for each experiment was kept 0.3 g. The dishes containing catalysts were dried in an oven at 100 °C for about 3 h to evaporate the water and then cooled to room temperature before used. After sample-coated dishes were placed

in the reactor, a small amount of acetone was injected into the reactor with a micro-syringe. The reactor was connected to a $CaCl_2$-containing dryer used for controlling the initial humidity in the reactor. The analysis of acetone, carbon dioxide, and water vapor concentration in the reactor was conducted online with a Photoacoustic IR Multigas Monitor (INNOVA Air Tech Instruments Model 1312). The acetone vapor was allowed to reach adsorption equilibrium with catalysts in the reactor prior to UV light irradiation. The initial concentration of acetone after adsorption equilibrium was controlled to 350 ± 10 ppm, which remained constant for about 5 min until a 15 W 365 nm UV lamp (6 cm above the dishes) in the reactor was turned on. Integrated UV intensity was measured with a UV radiometer (Model: UV-A, made in Photoelectric Instrument Factory of Beijing Normal University). Integrated UV intensity was 2.9 ± 0.1 mW/cm^2, while the peak wavelength of UV light was 365 nm. The initial concentration of water vapor was 1.20 ± 0.01 vol%, and the initial temperature was 30 ± 1 °C. Each set of experiment was followed for 60 min.

Since photocatalytic oxidation of acetone on the surface of TiO_2 powders is a pseudo-first-order reaction and its kinetic equation may be expressed as follows [31]:

$$r = -\frac{dc}{dt} = kKc = k_a c \quad (2)$$

where k_a is the apparent kinetic constant of pseudo-first order. So the concentration of gas will decrease following the arithmetical progression proportion. The rate equation is:

$$\ln \frac{c_0}{c_t} = k_a t \quad (3)$$

where c_0 and c_t are initial equilibrium concentration of the acetone and the reaction concentration of acetone, respectively.

3. Results and discussions

3.1. Thermal analysis

Fig. 1 shows DTA/TG curves of the US80-0.25 sample. It can be seen from DTA curve that a broad endothermic peak at below 100 °C is due to evaporation of the physically absorbed water and produced alcohol. There are three exothermic peaks at 224.5, 391.3 and 715.7 °C. The first one may be attributed to phase transformation of amorphous to anatase (see Fig. 3) [32–34]. The second one is probably due to the thermal decomposition of un-hydrolyzed alkyl or ferric nitrate [4]. The third one is due to phase transformation of anatase to rutile [4,11]. It can be concluded from DTA result that ultrasonic irradiation reduces the phase transformation temperatures of amorphous to anatase and anatase to rutile. Usually, the phase transitions from amorphous to anatase and anatase to rutile occur at about 400 and 900 °C, respectively [4]. The TG curve in Fig. 1 can be divided into two stages. The larger weight loss (25.5%) occurs in the temperature range from room temperature to 250 °C. This is attributed to the evaporation of the physically absorbed water and produced alcohol. The second stage is from 250 to 900 °C and a mass loss of about 1.64% is observed, which can be ascribed to the evaporation of a small amount of chemisorbed water.

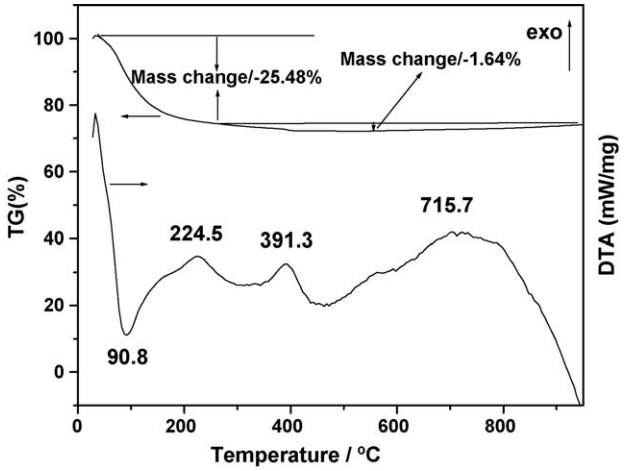

Fig. 1. DTA/TG curves of the US80-0.25 TiO_2 powders.

3.2. XRD study

XRD was used to investigate the phase structure and the phase composition of TiO_2 powders. Fig. 2 shows the effects of Fe-doped concentration on phase structures of the TiO_2 powders calcined at 400 °C. It can be seen that the diffraction peaks of all samples are the anatase phase. With Fe-doping concentration increasing, the peak intensities of anatase slightly decrease and the width of (1 0 1) plane diffraction peak of anatase ($2\theta = 25.4°$) becomes broader. Therefore, it is reasonable to deduce that the larger the amount of Fe-doping, the poorer the crystallization of the TiO_2 powders, and the smaller the crystallite size of TiO_2 (as shown in Table 1). It is interesting to note that iron oxides or Fe_xTiO_y phases are not found in the patterns of XRD, which is in accord with the results reported by Refs. [19,35]. There are two reasons responsible for this. One probable reason is that the concentration of Fe-doping is so low that it cannot be detected by XRD. The other is that the radii of Ti^{4+} (0.68 Å) and Fe^{3+} (0.64 Å) ions are very similar and all the iron ions maybe insert

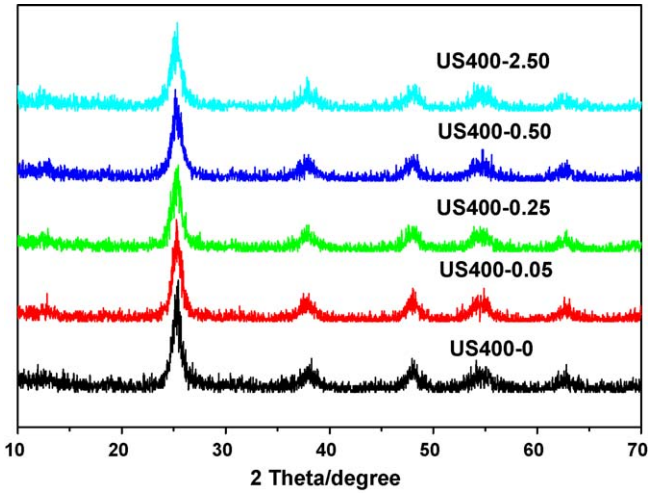

Fig. 2. XRD patterns of the TiO_2 powders prepared at different Fe-doping concentrations and calcined at 400 °C.

Table 1
Effects of Fe-doping concentration on physical properties of TiO_2 powders

Sample	Phase content[a]	Crystalline size[b] (nm)	Surface area[c] (m^2/g)	Pore volume[d] (cm^3/g)	Average pore[d] (size/nm)
US400-0	A	10.6 (1.00)	133.0	0.257	8.5
US400-0.05	A	9.9 (0.91)	144.6	0.307	8.5
US400-0.25	A	9.4 (0.81)	147.7	0.332	8.3
US400-0.50	A	8.7 (0.79)	155.3	0.383	7.7
US400-2.50	A	7.3 (0.77)	185.4	0.253	6.9
P25	A (80%) + R (20%)	30.0	63.0	0.060	3.8

[a] A and R denote anatase and rutile, respectively.
[b] Average crystalline size of TiO_2 was determined by XRD using Scherrer equation. Relative anatase crystallinity: the relative intensity of the diffraction peak from the anatase(1 0 1) plane (indicated in parentheses, reference = the US400-0 sample).
[c] The BET surface area was determined by multipoint BET method using the adsorption data in the relative pressure (P/P_0) range of 0.05–0.3.
[d] Pore volume and average pore size were determined by nitrogen adsorption volume at the relative pressure of 0.994.

into the structure of titanium, and locate at interstices or occupy some of the titanium lattice sites, forming an iron–titanium oxide solid solution [35].

Fig. 3 shows XRD patterns of the sample US80-0.25 calcined at different temperatures. It can be seen that the calcination temperatures obviously influence the crystallization. Before calcination, the as-prepared powders are amorphous, which is not agreement with our previous results [25]. This can be assigned to the fact that, in that work, TBOT was hydrolyzed at room temperature and the temperature of solution was steadily increased during the sonication. However, in the present work, the hydrolysis temperature always kept at about 20 °C. When the TBOT was hydrolyzed at 20 °C, the rate of hydrolysis would be slowed down and there were a large amount of un-hydrolyzed alkyls remaining in the xerogel powders. These un-hydrolyzed alkyls prevented the phase transformation of amorphous to anatase and the crystallization by adsorbing alkyls on the surfaces of TiO_2 particles. Consequently, the as-prepared TiO_2 xerogel powders were amorphous [29]. Moreover, the guest phase, Fe-doing also hindered the phase transformation of amorphous to anatase and the crystallization. With increasing calcination temperature, the diffraction peak intensities of anatase slightly increased and the width of the (1 0 1) plane diffraction peak of anatase ($2\theta = 25.4$) became narrower. At 600 °C, the average crystallite size of anatase reached 55.7 nm (as shown in Table 1). The rapid increase in the anatase crystalline size was attributed to the facts that high temperatures enhanced the growth of TiO_2 crystalline.

3.3. BET surface areas and other physical properties

Fig. 4 shows N_2 adsorption–desorption isotherms of the TiO_2 powders prepared at different Fe-doping concentration and calcined at 400 °C. All the powders show isotherms of type IV (BDDT classification) [26]. At high relative pressures from 0.45 to 0.95, the isotherms exhibit hysteresis loops of type H3, indicating that the powders contain mesopores (2–50 nm). The corresponding pore size distributions of the powders are shown in Fig. 5. It can be seen that the diameter ranges of pores locate from 1.5 to 10 nm and the average diameter of pores is about 7–8 nm (as shown in Table 1). The formation of mesoporous structure in the powders is attributed to the aggregation of TiO_2 crystallites [31]. With increasing Fe-doping concentration, the average pore size decreases slightly from 8.5 to 6.9 nm. There are two possible factors resulting in the decrease of pore size. One is that the aggregation of smaller crystallites forms smaller

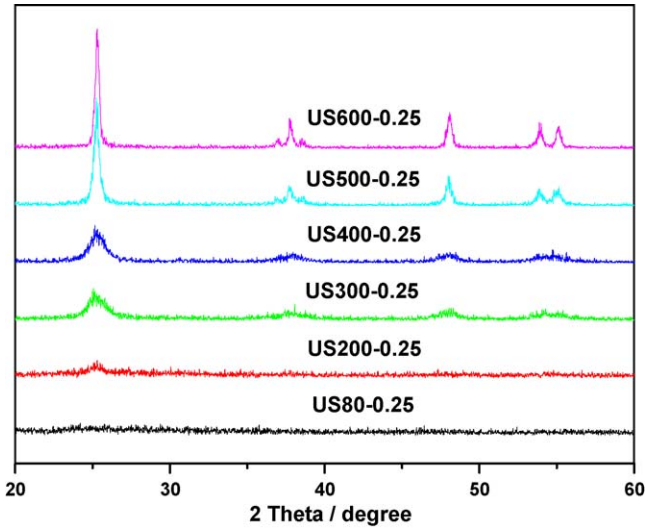

Fig. 3. XRD patterns of the TiO_2 powders prepared at a Fe/Ti atomic ratio of 0.25 (at.%) and calcined at different temperatures.

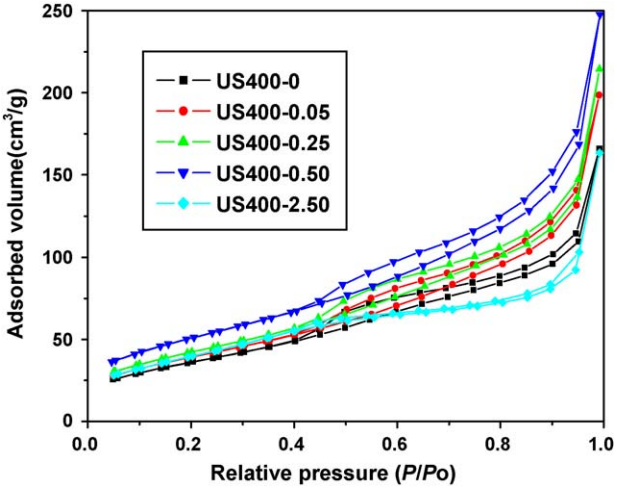

Fig. 4. N_2 adsorption–desorption isotherms of the TiO_2 powders prepared at different Fe-doping concentration and calcined at 400 °C.

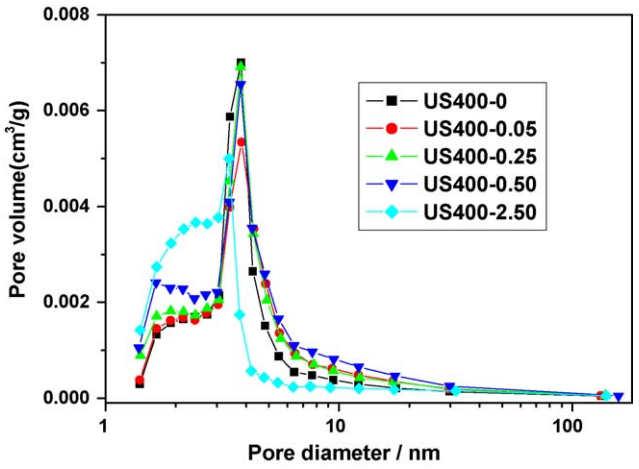

Fig. 5. Pore size distributions of the TiO_2 powders prepared at different Fe-doping concentration and calcined at 400 °C.

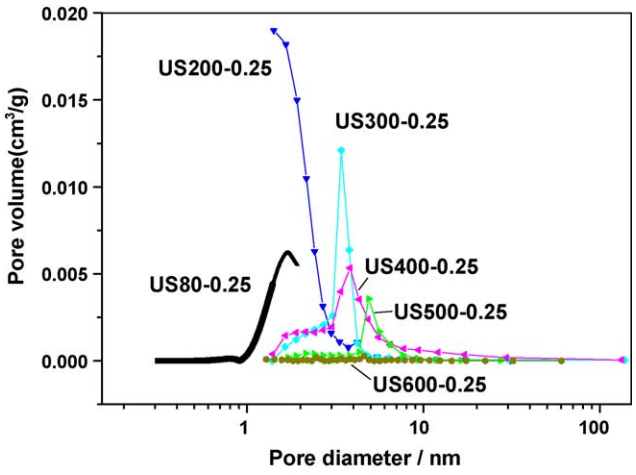

Fig. 7. Pore size distributions of the TiO_2 powders prepared at a Fe/Ti atomic ratio of 0.25 (at.%) and calcined at different temperatures.

pores. The other is that some Fe^{3+} ions of doping probably insert into the pore of pure TiO_2, which also causes pore size to become smaller [19].

Fig. 6 shows N_2 adsorption–desorption isotherms of the TiO_2 powders prepared at a Fe/Ti atomic ratio of 0.25 (at.%) and calcined at different temperatures. It can be seen that adsorption–desorption isotherms of the samples are obviously influenced by the calcination temperatures. Before calcination, the isotherm of the US80-0.25 sample was types I (BDDT classification), indicating that the powders contained micropores. While at 200 °C, the isotherm of the US200-0.25 sample is a combination of types I and IV with two very distinct regions: at low relative pressure, the isotherm exhibited high adsorption, indicating that the powder contained micropores (type I). However, at high relative pressure between 0.5 and 1.0, the curve exhibited a very small hysteresis loop, indicating the presence of mesopores (type IV). At 300, 400 and 500 °C, the isotherms of the US300-0.25, US400-0.25 and US500-0.25 samples exhibited a similar hysteresis loop at relative pressure between 0.5 and 1.0, indicating that the presence of mesopores. At 600 °C, the

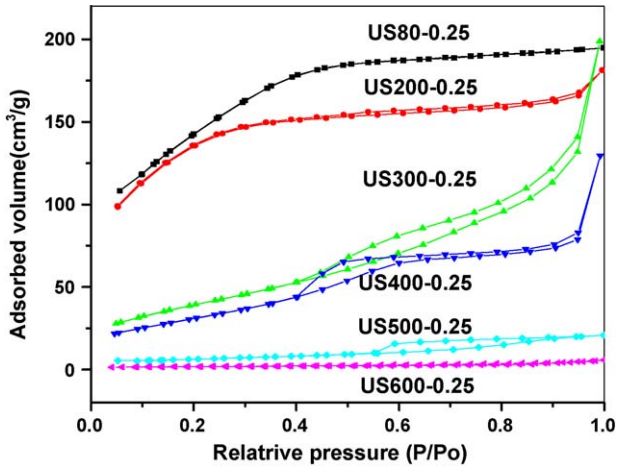

Fig. 6. N_2 adsorption–desorption isotherms of the TiO_2 powders prepared at a Fe/Ti atomic ratio of 0.25 (at.%) and calcined at different temperatures.

US600-0.25 sample almost had no hysteresis loop, indicating that all the pores collapse during the calcination and the total pore volume is very small.

Fig. 7 shows corresponding pore size distributions of the TiO_2 powders prepared at a Fe/Ti atomic ratio of 0.25 (at.%) and calcined at different temperatures. It can also be seen that calcination temperature significantly influences the pore size distribution of the TiO_2 powders. Before calcination, the US80-0.25 sample shows a typical micropore distribution determined via HK method. At 200 °C, the US200-0.25 sample has a wide pore size distribution from micropore to mesopore, but the portion of micropore is not shown here because of using the BJH method. With increasing calcination temperatures, the curves of the pore size distribution shift to the mesoporous region and the pore volumes decrease slowly. At 600 °C, the pore size distribution of the US600-0.25 sample turns into a line, indicating the disappearance of pores.

Table 1 shows the effects of Fe-doping concentration on the physical properties of TiO_2 powders. It can be seen that with increasing Fe-doping concentration, the specific surface areas of the samples increase from 133.0 to 185.4 m^2/g, while the average pore sizes decrease slightly from 8.5 to 6.9 nm, and the relative anatase crystallinity becomes poor. At the Fe/Ti atomic ratio = 2.50 (at.%), the relative anatase crystallinity of the US400-2.50 sample is about 77.0% of the US400-0 sample. Table 2 shows the effects of calcination temperatures on physical properties of TiO_2 powder. At 200 °C, the US200-0.25 sample turns into anatase phase from amorphous. With increasing calcination temperatures, the average crystallite sizes increase from 6.2 to 55.7 nm, the specific surface areas decrease abruptly from 511.1 to 5.6 m^2/g, and the pore volumes change from 0.302 to 0.001 cm^3/g. On the contrary, the relative anatase crystallinity increases from 0.46 of the US200-0.25 sample to 3.16 of the US600-0.25 sample.

3.4. UV–visible absorbance spectra

Usually, metal ions doping obviously affects light absorption characteristics of TiO_2 [36–40]. Fig. 8 shows UV–vis

Table 2
Effects of calcined temperature on physical properties of TiO_2 powders

Sample	Phase content[a]	Crystallite size[b] (nm)	Surface area[c] (m^2/g)	Pore volume[d] (cm^3/g)	Average pore size[d] (nm)
US80-0.25	Am	–	511.1	0.302	2.3
US200-0.25	A	6.2 (0.46)	284.9	0.426	6.0
US300-0.25	A	8.7 (0.63)	144.6	0.307	7.0
US400-0.25	A	9.4 (1.00)	147.7	0.332	8.3
US500-0.25	A	26.5 (2.86)	22.3	0.030	5.8
US600-0.25	A	55.7 (3.16)	5.6	0.001	7.0

[a] A and Am denote anatase and amorphous, respectively.
[b] Average crystalline size of TiO_2 was determined by XRD using Scherrer equation. Relative anatase crystallinity: the relative intensity of the diffraction peak from the anatase(1 0 1) plane (indicated in parentheses, reference = the US400-0.25 sample).
[c] The BET surface area was determined by multipoint BET method using the adsorption data in the relative pressure (P/P_0) range of 0.05–0.3.
[d] Pore volume and average pore size were determined by nitrogen adsorption volume at the relative pressure of 0.994.

absorbance spectra of the Fe-doped TiO_2 powders prepared at different Fe-doping concentration and calcined at 400 °C. A significant increase in the absorption at wavelengths shorter than 400 nm can be assigned to the intrinsic band gap absorption of TiO_2. The absorption spectra of the Fe-doped TiO_2 samples show a stronger absorption in the UV–visible light region and an obvious red shift in the band gap transition. Generally, the photocatalytic activity is proportional to $(I_\alpha\phi)^n$ ($n = 1$ for low light intensity and $n = 1/2$ for high light intensity), where I_α is the photo numbers absorbed by photocatalyst per second and ϕ is the efficiency of the band gap transition. The enhancement of the photoactivity for Fe-doped TiO_2 powders can be partly explained in terms of an increase in $I_\alpha\phi$, resulting from intensive absorbance in the UV–visible region [2,20]. Fe-doping obviously affects light absorption characteristics of TiO_2 as shown in Fig. 8. With increasing Fe-doping concentration, the samples show a stronger absorption in the visible range and a red shift in the band gap transition. The red shift is ascribed to the results of the Fe-doping.

The absorption edges shift toward longer wavelengths for the Fe-doped TiO_2 powders. This clearly indicates a decrease in the band gap energy of TiO_2. The direct band gap energy can be estimated from a plot of $(\alpha h\nu)^2$ versus photon energy ($h\nu$). The intercept of the tangent to the plot will give a good approximation of the band gap energy for TiO_2. The absorption coefficient α can be calculated from the measured absorbance (A) according to the Refs. [41,42]. Plots of the $(\alpha h\nu)^2$ versus photon energy ($h\nu$) are shown in Fig. 9. The band gap energies estimated from the intercept of the tangents to the plots are 3.24, 3.18, 3.13, 3.02 and 2.71 eV for different doping concentration at 0, 0.05, 0.25, 0.50, and 2.50 at.%, respectively. The band gap energies decrease with increasing Fe-doping concentration. This indicates that Fe-doping probably influences the photocatalytic activity of TiO_2.

3.5. XPS

In order to identify the chemical status of Fe in the Fe-doped TiO_2 samples, Fig. 10 shows the high-resolution XPS spectra of the Fe2p region of the US400-0.25 and US400-2.50 samples. It can be found that the peaks of $Fe2p_{3/2}$ can be decomposed into two contributions corresponding to the different oxidation of iron, respectively. The main contribution is attributed to Fe^{3+} ions (binding energy at 709.1 eV), and the other is to Fe^{2+} ion (binding energy at 710.9 eV) [43,44]. Further XPS studies showed that all Fe-doped TiO_2 powders contained Fe^{3+} and Fe^{2+} ions. The formation of a small amount of Fe^{2+} ions in the TiO_2 powders could be ascribed to the presence of residual carbon in

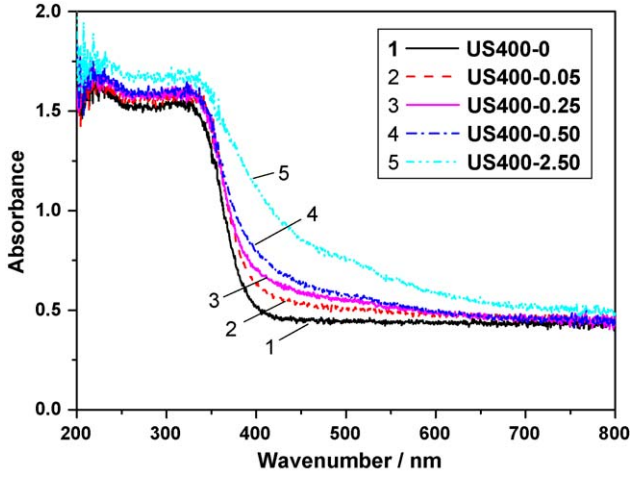

Fig. 8. UV–vis absorbance spectra of Fe-doped TiO_2 powders prepared at different Fe-doping concentration and calcined at 400 °C.

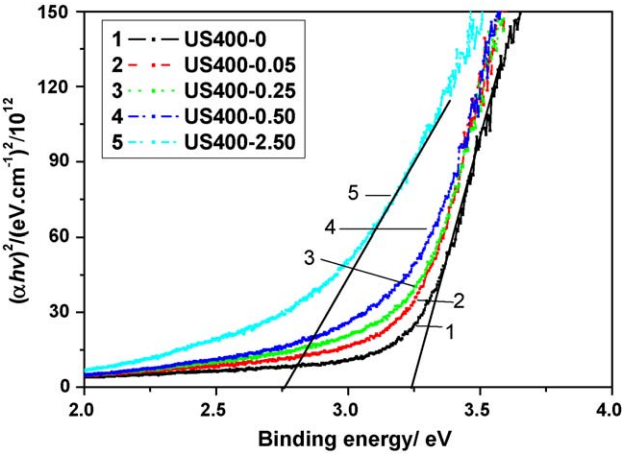

Fig. 9. Plots of the $(\alpha h\nu)^2$ vs. photon energy ($h\nu$) of Fe-doped TiO_2 powders prepared at different Fe-doping concentration and calcined at 400 °C.

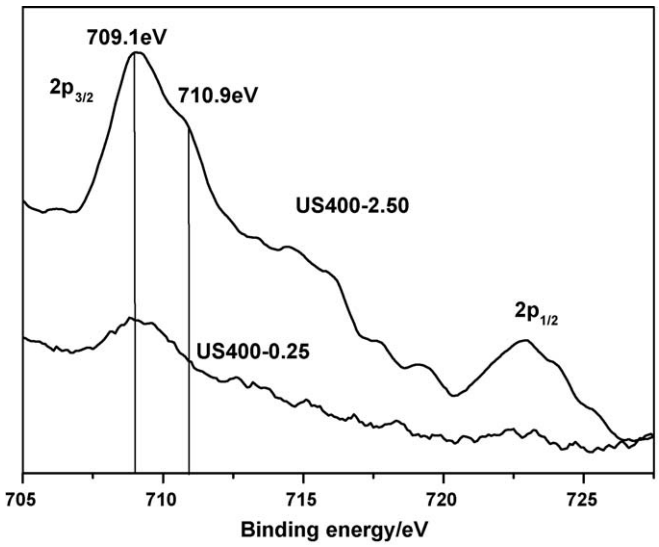

Fig. 10. High-resolution XPS spectra of the Fe2p region of the US400-0.25 and US400-2.50 samples.

the TiO_2 powders from organic radicals introduced by molecular precursors. During thermal treatment at 400 °C, the oxidation of carbon would draw oxygen from the surrounding atmosphere and Fe–O network, resulting in the reduction of Fe^{3+} to Fe^{2+} [19].

3.6. Photocatalytic activity

Fig. 11 shows effect of Fe-doping concentration on apparent kinetic constants (min^{-1}) of the Fe-doped TiO_2 powders calcined at 400 °C. It can be seen that the apparent kinetic constant of the US400-0 sample (without Fe-doping) prepared by ultrasonic method has the decent photocatalytic activity. When a small amount of Fe (0.05 at.%) is doped into TiO_2 powders, the photocatalytic activity of the prepared samples increases slightly. At Fe/Ti atomic ration = 0.25 (at.%), the photocatalytic activity of the US400-0.25 sample reaches a maximum value, and its activity exceeds that of Degussa P25 by a factor of more than two times. With further increasing Fe-doping concentration, the phtotcatalytic activity of the powders decreases obviously. The high phtotcatalytic activity of the US400-0.25 sample is due to the following several factors.

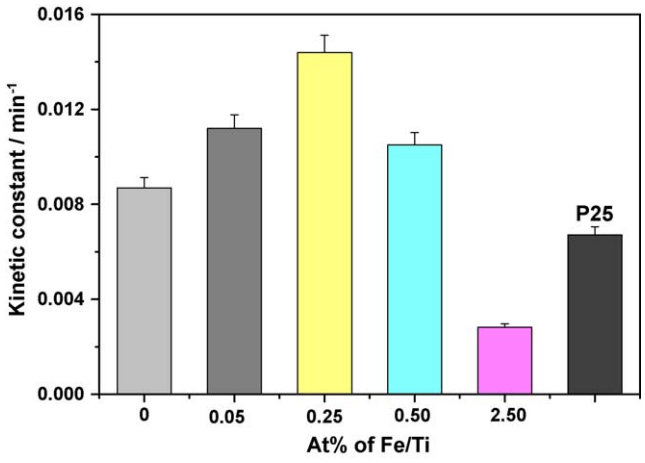

Fig. 11. The apparent kinetic constants (min^{-1}) vs. the Fe-doped TiO_2 powders prepared at different Fe-doping concentration and calcined at 400 °C.

Firstly, Fe^{3+} ions can enhance the intensity of absorption in the UV–visible light region and make a red shift in the band gap transition of the Fe-doped TiO_2 samples. This can induce more photo-generated electrons and holes to participate in the photocatalytic reactions. Apart from this effect, Fe^{3+} ions can also serve as a mediator of the transfer of interfacial charge at an appropriate doping concentration. The activity evaluation shows that the presence of a small amount of Fe^{3+} ions can enhance the activity, but excessive Fe^{3+} ions are detrimental. This may be due to the fact that a small amount of Fe^{3+} ions can act as a photo-generated hole and a photo-generated electron trap and inhibit the hole–electron recombination [19,35]:

$$TiO_2 + h\nu \rightarrow h^+ + e^- \text{ (charge pair generation)} \quad (4)$$

$$Ti^{4+} + e^- \rightarrow Ti^{3+} \quad (5)$$

$$O^{2-} + h^+ \rightarrow O^- \quad (6)$$

$$Fe^{3+} + Ti^{3+} \rightarrow Fe^{2+} + Ti^{4+} \text{ (electron trap)} \quad (7)$$

$$Fe^{3+} + O^- \rightarrow Fe^{4+} + O^{2-} \text{ (hole trap)} \quad (8)$$

From the viewpoint of crystal field theory, Fe^{4+} and Fe^{2+} ions are relatively unstable as compared to Fe^{3+} ions, which have half-filled d orbital (d^5). Therefore, there is a tendency for the transfer of the trapped charges from Fe^{4+} and Fe^{2+} to the interface to initiate the following reactions [19]:

$$Fe^{4+} + OH^- \rightarrow Fe^{3+} + OH^{\bullet} \text{ (hole release)} \quad (9)$$

$$Fe^{2+} + O_2 \rightarrow Fe^{3+} + O_2{}^- \text{ (electron release)} \quad (10)$$

As a result, the introduction of Fe^{3+} ions in TiO_2 powder is responsible for a reduction in the photo-generated hole–electron recombination rate. Moreover, a decrease in the activity is expected when the concentration of Fe^{3+} ions becomes too large. Many investigations have shown that the photocatalytic activity of Fe-doped TiO_2 is strongly dependent on the dopant concentration since the Fe^{3+} ions can serve not only as a mediator of interfacial charge transfer but also as a recombination center. In our case an optimal dopant concentration is 0.25 at.%. Above that concentration, Fe^{3+} ions steadily become recombination centers and the activity steadily decreases. When the dopant concentration reaches 2.50 at.%, Fe^{3+} ions mainly act as recombination centres through quantum tunneling [15,45]. Therefore, the activity of the US400-2.50 sample becomes the lowest and only 30% of the un-doped powder. Furthermore, it is commonly accepted that a narrower band gap corresponds to less powerful redox ability. Because the photocatalytic process system can be considered similar to an electrochemical cell, the decrease in band gap results in a lower oxidation–reduction potential based on the equation [46]:

$$\Delta G = -nFE \quad (11)$$

ΔG is the free energy change of the redox process occurring in the system, n the number of moles of electrons transferred

involved in the process of redox, F the Faraday constant and E represents the band gap of the semiconductor. This also indicates that the band gap narrowing resulting from the Fe-doping cannot always be a favorable factor for the photocatalytic activity. So an optimal dopant concentration is needed for the doping of TiO_2.

Secondly, a large surface area may be a important factor in certain photocatalytic degradation reactions, as a large amount of adsorbed organic molecules promotes the reaction rate [19,25]. However, powders with a large surface area are usually associated with large amounts of crystalline defects, which favor the recombination of photo-generated electrons and holes leading to a poor photoactivity [5,47,48]. So the large surface area is a requirement, but not a decisive factor. Usually, the photocatalytic activity of amorphous TiO_2 is negligible, also indicating that crystallinity is another important requirement [5,49]. So a balance between specific surface area and crystallinity is a very important factor in determining the photocatalytic activity of TiO_2 powders. According to above results and discussion, the US400-0.25 sample prepared by the ultrasonic method possesses relative large surface area and good anatase crystallinity (as shown in Table 1), resulting in a good photocatalytic activity.

Thirdly, particle size is another important parameter influencing photocatalytic efficiency, since the electron–hole recombination rate may depend on the particle size. It is well known that in the nanometer-size range, physical and chemical properties of semiconductors are modified (compared with bulk). Small variations in particle diameters lead to great modifications in the surface/bulk ratio, thus influencing the recombination rates of volume and surface electrons and holes. Some investigation reported that the anatase TiO_2 quantum yield for photocatalytic reaction also increased with decreasing particle size [5,48,50]. Especially in the range of less than 10 nm, a significant increasing of the quantum yields was observed due to the fact that for the photo-generated electrons and holes, the average diffusion time from the bulk to the surface could be estimated by the formula:

$$\tau = \frac{r^2}{\pi^2 D} \tag{12}$$

where r is the particle radius and D is the diffusion coefficient of the carriers (to the diffusion coefficient of conduction band electrons in TiO_2, the value of De^- is about 2×10^{-2} cm^2/s) [42]. So it can be predicted that the average transfer time of the US400-0.25 sample is only about 10% of that of Degussa P25. Therefore, the recombination rate of photo-generated electrons and holes will be drastically decreased and the photocatalytic activity of the samples probably increases.

Many studies have shown that calcination is an effective treatment method to enhance the photoactivity and crystallization of nanosized TiO_2 photocatalysts [49,51–53]. Fig. 12 shows the effect of calcination temperature on apparent kinetic constants (min^{-1}) of the TiO_2 powders prepared at a Fe/Ti atomic ratio of 0.25 (at.%). Before calcination, there is a very low photocatalytic activity observed for the US80-0.25 sample, which is due to the fact the powders are composed of amorphous TiO_2. With increasing calcination temperatures, the apparent kinetic constants increase. The enhancement of photocatalytic activity at elevated temperatures can be ascribed to an obvious improvement in crystallization or relative anatase crystallinity (as shown in Table 2). The US300-0.25 sample shows a good photocatalytic activity due to the formation of anatase phase. At 400 °C, the apparent kinetic constant of the samples reaches a maximum value of $k = 0.0144$. The value of k is more than two times higher than that of P25 ($k = 0.0061$). The high photocatalytic activity of the US400-0.25 sample is due to its relative large surface area, small crystallite size and good crystallization. At a higher temperature, the apparent kinetic constants decrease rapidly and reach a minimum value of 0.0009 at 600 °C due to drastic decrease in specific surface areas and pore volume.

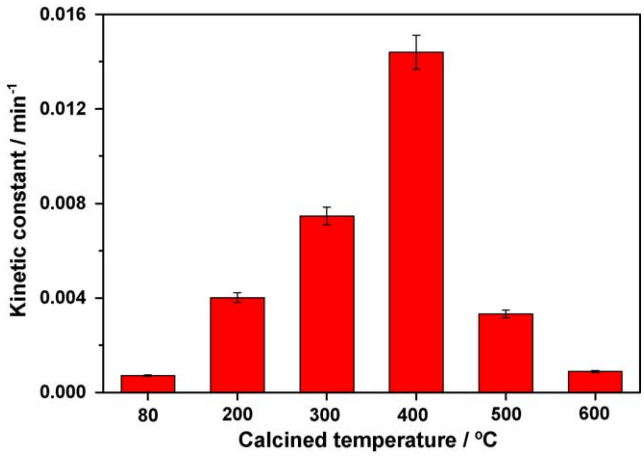

Fig. 12. The apparent kinetic constants (min^{-1}) vs. the calcined TiO_2 powders prepared at a Fe/Ti atomic ratio of 0.25 (at.%) and calcined at different temperatures.

4. Conclusions

Highly active nanocrystalline mesoporous Fe-doped TiO_2 photocatalysts could be prepared by an ultrasonic-induced hydrolysis reaction of tetrabutyl titanate ($Ti(OC_4H_9)_4$) in a ferric nitrate aqueous solution. The Fe-doped TiO_2 powders showed a strong absorption in the UV–visible light region and a red shift in the band gap transition.

A small amount of Fe-doping could obviously enhance the photocatalytic activity of TiO_2 powders. At an optimal atomic ratio of Fe to Ti of 0.25, the photocatalytic activity of Fe-doped TiO_2 powders prepared by this method and calcined at 400 °C exceeded that of Degussa P25 (P25) by a factor of more than two times. The high activities of the Fe-doped TiO_2 powders could be attributed to the results of the synergetic effects of Fe-doping, large BET specific surface area and small crystallite size.

Acknowledgements

This work was partially supported by the National Natural Science Foundation of China (20473059). This work was also financially supported by the Key Research Project of the Ministry of Education (No. 106114).

References

[1] H. Tada, M. Yamamoto, S. Ito, Promoting effect of MgO_x submonolayer coverage of TiO_2 on the photoinduced oxidation of anionic surfactants, Langmuir 15 (1999) 3699.

[2] M.R. Hoffmann, S.T. Martin, W. Choi, D.W. Bahnemann, Environmental applications of semiconductor photocatalysis, Chem. Rev. 95 (1995) 69.

[3] A. Fujishima, T.N. Rao, D.A. Tryk, Titanium dioxide photocatalysis, J. Photochem. Photobiol. C 1 (2000) 1.

[4] J.G. Yu, J.C. Yu, W.K. Ho, M.K.P. Leung, B. Cheng, G.K. Zhang, X.J. Zhao, Effects of alcohol content and calcination temperature on the textural properties of bimodally mesoporous titania, Appl. Catal. A 255 (2003) 309.

[5] O. Carp, C.L. Huisman, A. Reller, Photoinduced reactivity of titanium dioxide, Prog. Solid State Chem. 32 (2004) 33.

[6] W. Huang, X. Tang, I. Felner, Y. Koltypin, A. Gedanken, Preparation and characterization of Fe_xO_y–TiO_2 via sonochemical synthesis, Mater. Res. Bull. 37 (2002) 1721.

[7] J.A. Wang, R.L. Ballesteros, T. Lopez, A. Moreno, R. Gomez, O. Novaro, X. Bokhimi, Quantitative determination of titanium lattice defects and solid-state reaction mechanism in iron-doped TiO_2 photocatalysts, J. Phys. Chem. B 105 (2001) 9692.

[8] F.B. Li, X.Z. Li, M.F. Hou, Photocatalytic degradation of 2-mercaptobenzothiazole in aqueous La^{3+}–TiO_2 suspension for odor control, Appl. Catal. B 48 (2004) 185.

[9] F.B. Li, X.Z. Li, Photocatalytic properties of gold/gold ion-modified titanium dioxide for wastewater treatment, Appl. Catal. A 228 (2002) 15.

[10] X.T. Hong, Z.P. Wang, W.M. Cai, F. Lu, J. Zhang, Y.Z. Yang, N. Ma, Y.J. Liu, Visible-light-activated nanoparticle photocatalyst of iodine-doped titanium dioxide, Chem. Mater. 17 (2005) 1548.

[11] J.C. Yu, J.G. Yu, W.K. Ho, Z.T. Jiang, L.Z. Zhang, Effects of F^- doping on the photocatalytic activity and microstructures of nanocrystalline TiO_2 powders, Chem. Mater. 14 (2002) 3808.

[12] J.G. Yu, J.F. Xiong, B. Cheng, Y. Yu, J.B. Wang, Hydrothermal preparation and visible-light photocatalytic activity of Bi_2WO_6 powders, J. Solid State Chem. 178 (2005) 1968.

[13] J. Ovenstone, Preparation of novel titania photocatalysts with high activity, J. Mater. Sci. 36 (2001) 1325.

[14] J. Soria, J.C. Conesa, V. Augugliaro, L. Palmisano, M. Schiavello, A. Sclafani, Dinitrogen photoreduction to ammonia over titanium dioxide powders doped with ferric ions, J. Phys. Chem. 95 (1991) 274.

[15] W. Choi, A. Termin, M.R. Hoffmann, The role of metal ion dopants in quantum-sized TiO_2: correlation between photoreactivity and charge carrier recombination dynamics, J. Phys. Chem. 98 (1994) 13669.

[16] J. Moon, H. Takagi, Y. Fujishiro, M. Awano, Preparation and characterization of the Sb-doped TiO_2 photocatalysts, J. Mater. Sci. 36 (2001) 949.

[17] T. Ohno, T. Tsubota, M. Toyofuku, R. Inaba, Photocatalytic activity of a TiO_2 photocatalyst doped with C^{4+} and S^{4+} ions having a rutile phase under visible light, Catal. Lett. 98 (2004) 255.

[18] T. Ohno, M. Akiyoshi, T. Umebayashi, K. Asai, T. Mitsui, M. Matsumura, Preparation of S-doped TiO_2 photocatalysts and their photocatalytic activities under visible light, Appl. Catal. A 265 (2004) 115.

[19] M.H. Zhou, J.G. Yu, B. Cheng, H.G. Yu, Preparation, Photocatalytic activity of Fe-doped mesoporous titanium dioxide nanocrystalline photocatalysts, Mater. Chem. Phys. 93 (2005) 159.

[20] C.Y. Wang, D.W. Bahnemann, J.K. Dohrmann, A novel preparation of iron-doped TiO_2 nanoparticle with enhanced photocatalytic activity, Chem. Commun. (2000) 1539.

[21] A. Gedanken, X. Tang, Y. Wang, N. Perkas, Y. Koltypin, N. Perkas, Y. Koltypin, M.V. Landau, L. Vradman, M. Herskowitz, Using sonochemical methods for the preparation of mesoporous materials and for the deposition of catalysts into the mesopores, Chem. Eur. J. 2 (2001) 4547.

[22] G. Dantsin, K.S. Suslick, Sonochemical preparation of a nanostructured bifunctional catalyst, J. Am. Chem. Soc. 122 (2000) 5214.

[23] N. Perkas, O. Palchik, I. Brukental, I. Nowik, Y. Gofer, Y. Koltypin, A. Gedanken, A mesoporous iron–titanium oxide composite prepared sonochemically, J. Phys. Chem. B 107 (2003) 8772.

[24] K.S. Suslick, S.B. Choe, A.A. Cichowlas, M.W. Grinstaff, Sonochemical synthesis of amorphous iron, Nature 353 (1991) 414.

[25] J.G. Yu, M.H. Zhou, B. Cheng, H.G. Yu, X.J. Zhao, Ultrasonic preparation of mesoporous titanium dioxide nanocrystalline photocatalysts and evaluation of photocatalytic activity, J. Mol. Catal. A 227 (2005) 75.

[26] S.W. Sing, D.H. Everett, R.A.W. Haul, L. Moscou, R.A. Pierotti, J. Rouquerol, T. Siemieniewska, Reporting physisorption data for gas/solid systems with special reference to the determination of surface area and porosity, Pure Appl. Chem. 57 (1985) 603.

[27] M.E. Zorn, D.T. Tompkins, W.A. Zeltner, M.A. Anderson, Photocatalytic oxidation of acetone vapor on TiO_2/ZrO_2 thin films, Appl. Catal. B 23 (1999) 1.

[28] Y. Sekine, Oxidative decomposition of formaldehyde by metal oxides at room temperature, Atm. Environ. 36 (2002) 5543.

[29] J.G. Yu, J.C. Yu, B. Cheng, X.J. Zhao, Preparation and characterization of highly photoactive nanocrystalline TiO_2 powders by solvent evaporation-induced crystallization method, Sci. China B 46 (2003) 549.

[30] J.C. Yu, J.G. Yu, W.K. Ho, L.Z. Zhang, Preparation of highly photocatalytic active nano-sized TiO_2 particles via ultrasonic irradiation, Chem. Commun. (2001) 1942.

[31] M.M. Rahman, K.M. Krishna, T. Soga, T. Jimbo, M. Umeno, Optical properties and X-ray photoelectron spectroscopic study of pure and Pb-doped TiO_2 thin film, J. Phys. Chem. Solids 60 (1999) 201.

[32] J.G. Yu, J.C. Yu, B. Cheng, S.K. Hark, K. Iu, The effect of F^--doping and temperature on the structural and textural evolution of mesoporous TiO_2 powders, J. Solid State Chem. 174 (2003) 372.

[33] J.G. Yu, J.C. Yu, W.K. Ho, Z.T. Jiang, Effects of calcination temperature on the photocatalytic activity and photo-induced super-hydrophilicity of mesoporous TiO_2 thin films, New J. Chem. 26 (2002) 607.

[34] J.C. Yu, J.G. Yu, L.Z. Zhang, W.K. Ho, Light-induced super-hydrophilicity and photocatalytic activity of mesoporous TiO_2 thin films, J. Photochem. Photobiol. A 148 (2002) 263.

[35] C.Y. Wang, C. Bottcher, D.W. Bahnemann, J.K. Dohrmann, Sol–gel synthesis and magnetic studies of titanium dioxide doped with 10% M (M = Fe, Mn and Ni), J. Mater. Chem. 13 (2003) 2322.

[36] A. Hattori, K. Shimoda, H. Tada, S. Ito, Photoreactivity of sol–gel TiO_2 films formed on soda-lime glass substrates: effect of SiO_2 underlayer containing fluorine, Langmuir 15 (1999) 5422.

[37] J.S. Park, W. Choi, Enhanced remote photocatalytic oxidation on surface-fluorinated TiO_2, Langmuir 20 (2004) 11523.

[38] R. Asahi, T. Morikawa, T. Okwaki, K. Aoki, Y. Taga, Visible-light photocatalysis in nitrogen-doped titanium oxides, Science 293 (2001) 269.

[39] W. Zhao, W. Ma, C. Chen, J. Zhao, Z. Shuai, Efficient degradation of toxic organic pollutants with Ni_2O_3/$TiO_{2-x}B_x$ under visible irradiation, J. Am. Chem. Soc. 126 (2004) 4782.

[40] T. Tachikawa, S. Tojo, K. Kawai, M. Endo, M. Fujitsuka, T. Ohno, K. Nishijima, Z. Miyamoto, T. Majima, Photocatalytic oxidation reactivity of holes in the sulfur- and carbon-doped TiO_2 powders studied by time-resolved diffuse reflectance spectroscopy, J. Phys. Chem. B 108 (2004) 19299.

[41] C. Kormann, D.W. Bahnemann, M.R. Hoffmann, Preparation and characterization of quantum-size titanium dioxide, J. Phys. Chem. 92 (1988) 5196.

[42] G. Rothenberger, J. Moser, M. Graetzel, N. Serpone, D.K. Sharma, Charge carrier trapping and recombination dynamics in small semiconductor particles, J. Am. Chem. Soc. 107 (1985) 8054.

[43] J.G. Yu, H.G. Yu, C.H. Ao, S.C. Lee, J.C. Yu, W.K. Ho, Preparation, characterization and photocatalytic activity of in situ Fe-doped TiO_2 thin films, Thin Solid Films 496 (2006) 273.

[44] W. Zhang, Y. Li, S. Zhu, F. Wang, Surface modification of TiO_2 film by iron doping using reactive magnetron sputtering, Chem. Phys. Lett. 373 (2003) 333.

[45] Z. Zhang, C.C. Wang, R. Zakaria, J.Y. Ying, Role of particle size in nanocrystalline TiO_2-based photocatalysts, J. Phys. Chem. B 102 (1998) 10871.

[46] J.C. Yu, L.Z. Zhang, J.G. Yu, Direct sonochemical preparation and characterization of highly active mesoporous TiO_2 with a bicrystalline framework, Chem. Mater. 14 (2002) 4647.
[47] K. Tanaka, M.F.V. Capule, T. Hisanaga, Effect of crystallinity of TiO_2 on its photocatalytic action, Chem. Phys. Lett. 187 (1991) 73.
[48] B. Ohtani, Y. Ogawa, S.I. Nishimoto, Photocatalytic activity of amorphous-anatase mixture of titanium(IV) oxide particles suspended in aqueous solutions, J. Phys. Chem. B 101 (1997) 3746.
[49] M. Anpo, T. Shima, S. Kodama, Y. Kubokawa, Photocatalytic hydrogenation of propyne with water on small-particle titania: size quantization effects and reaction intermediates, J. Phys. Chem. 91 (1987) 4305.
[50] P.G.F. Bisling, E. Ruehl, B. Brutschy, H. Baumgaertel, Photoionization mass spectroscopy with synchrotron radiation of hydrogen-bonded alkylamine clusters produced in supersonic beams, J. Phys. Chem. 91 (1987) 4310.
[51] M. Mrowetz, W. Balcerski, A.J. Colussi, M.R. Hoffmann, Oxidative power of nitrogen-doped TiO_2 photocatalysts under visible illumination, J. Phys. Chem. B 108 (2004) 17269.
[52] H. Kominami, S. Murakami, M. Kohno, Y. Kera, K. Okada, B. Ohtani, Stoichiometric decomposition of water by titanium(IV) oxide photocatalyst synthesized in organic media: effect of synthesis and irradiation conditions on photocatalytic activity, Phys. Chem. Chem. Phys. 3 (2001) 4102.
[53] Y. Tanaka, M. Suganuma, Effects of heat treatment on photocatalytic property of sol–gel derived polycrystalline TiO_2, J. Sol–Gel Sci. Technol. 22 (2001) 83.